Int J Adv Manuf Technol (2017) 88:2507–2516
DOI 10.1007/s00170-016-8972-y

ORIGINAL ARTICLE

Comprehensive thermal growth compensation method of spindle and servo axis error on a vertical drilling center

Kuo Liu[1] · **Yu Liu**[2] · **Ming-jia Sun**[3] · **Yu-liang Wu**[3] · **Tie-jun Zhu**[3]

Received: 11 March 2016 / Accepted: 25 May 2016 / Published online: 2 June 2016

Abstract This paper deals with the modeling of comprehensive thermal growth of spindle and servo axis. Thermal errors of a vertical drilling center TC500 were measured using a spindle error analyzer and a laser interferometer, thermal error of servo axis was decomposed, and each term analyzed. Spindle thermal growth model based on temperature variation including an identification method for the parameters of the suggested model was presented. Similarly, the servo axis models for thermal expansion error (TEE) in the stroke range and the thermal drift error (TDE) of origin were derived based on heat-transfer mechanism, and the parameter identification method was presented. The experimental results indicate that by applying the proposed model, high accuracy stability can be achieved, even when the moving state changes randomly. A specific machining process of the upper surface of a rectangular workpiece was designed to verify the effects of error compensation to the unaided eye. The machining results indicate that the proposed model has high accuracy and strong robustness in compensating the comprehensive thermal error.

Keywords Vertical drilling center · Spindle · Servo axis · Comprehensive thermal growth · Compensation

Highlights • The model based on temperature variation for thermal growth of spindles was designed.
• The change in velocity and acceleration of temperature was used for calculating the real-time steady value of the spindle thermal growth.
• The comprehensive thermal errors of a servo axis were divided into thermal expansion error (TEE) in the stroke range and the thermal drift error (TDE) of origin. The servo axis models for TEE and TDE were derived based on heat-transfer mechanism, and the parameter identification method was presented.
• A specific machining process of the upper surface of a rectangular workpiece was designed to check the effects of error compensation to the unaided eye.
• The experimental and machining results indicated that by applying the proposed model, high accuracy stability could be achieved, even when the moving state was changed randomly.

✉ Kuo Liu
liukuo0727@qq.com

[1] College of Mechanical Science and Engineering, Jilin University, Changchun 130025, People's Republic of China

[2] School of Mechanical Engineering and Automation, Northeastern University, Shenyang 110819, People's Republic of China

[3] State Key Laboratory, Shenyang Machine Tool (Group) CO., LTD., Shenyang 110142, People's Republic of China

1 Introduction

Thermal error accounts for approximately 40–70 % of the total errors of a machine tool [1–4], and it is the most relevant factor influencing the machine tool accuracy. The commonly used methods to minimize thermal errors are error avoidance and error compensation [5]. Error avoidance is to eliminate or reduce thermal errors by optimizing the mechanical design and construction phases of the machine tools, such as controlling the rate of temperature rise of heat source or the equilibrium temperature field, the symmetric design of the machine, and the adoption of a cooling system. Although this method increases the machine tool accuracy, production costs will dramatically increase. Therefore, the error avoidance technique may be an effective but not a cost-efficient method to enhance machine accuracy. On the other hand, the error compensation method is a "soft technique" that generates an opposite error that will eliminate the original thermal error. The error compensation method has many advantages, such as a wide field of applications at a lower cost than other does.

Thermal error of a machine tool mainly includes spindle thermal error and servo axes thermal errors. Among sources of

spindle thermal error, bearing rotation, motor heating, and the effect of environmental temperature are known to be key contributors. Similarly contribute to servo axis thermal errors the friction between the nut and screw, the rotation of the bearings and changes in environmental temperature. The spindle thermal error and the servo axes thermal errors are both significant and cannot be ignored. Because of small thermal deformations of the column, skate, and bed, the thermal error of the machine tool can be approximately treated as the superposition of these two kinds of errors. Various thermal error compensation methods have been widely studied in the past decades. Modeling methods for spindle thermal error include the multiple regression method [6, 7], Grey model [8, 9], time series method [10, 11], and neural network method [12]. Modeling methods for servo axes thermal errors include the multiple regression method [13, 14], neural network method [15, 16], and support vector machine method [17].

However, the aforementioned error modeling methods present following drawbacks: (1) Limitations. For example, a neural network model can only be efficient by using complete input and output data and that condition is hard to meet. Moreover, mistakes may occur by improperly choosing input and output training data. Grey model requires strictly smooth error data for modeling, while the time series method requires testing data under various speeds to establish a good model and a long time is needed. (2) Poor robustness. When the moving speed and range during actual machining differ from the thermal investigation, the predicted result becomes always poor, especially for multiple regression method. (3) Practical challenges. Some methods require many sensors to achieve high accuracy, thus being relatively expensive. Moreover, methods that require nut temperature measurements have significant risk of sensor failure. (4) Most studies focused on the spindle thermal error or on the servo axes thermal expansion error (TEE), and the thermal drift error (TDE) of origin and the comprehensive errors of spindle and servo axis have been rarely studied.

None of the aforementioned models is flawless; thus, the comprehensive axial thermal growth of spindle and Z-axis is studied on a vertical drilling center. The models for comprehensive thermal growth are proposed and validated through both experimental and machining tests.

2 Thermal error tests

The thermal growths of the spindle and of the servo axis were tested on a vertical drilling center TC500 featured with FANUC 0*i*-MD control. The maximum rotational speed of spindle was 24,000 rpm; the maximum speed of Z-axis was 48 m/min. Besides, Z-axis was half-closed-loop control type without cooling, with the ball screw fixed at one end and free at the other end.

Three temperature sensors (accuracy of ±0.1 °C) were placed on the outer surface of the front bearing of spindle, on the column, and on the Z-axis bearing block, respectively. The sensor was developed independently; the sensor chip was the TSictm-506F (IST Corporation, Switzerland). The cover of the sensor was magnetic. Due to its sensitivity to thermal growth of spindle, the temperature T_{sb} on the outer surface of the front bearing of spindle was chosen as the temperature reference index of spindle. The temperature T_b represents the temperature variation mainly caused by environment, and it mainly indicates TEE of servo axis caused by environment temperature variation and the environment temperature exchanging with screw. The temperature T_{br} represents the bearing block temperature variation mainly caused by screw rotation, and it mainly indicates TDE of servo axis. Figure 1 shows the positions of the three sensors on the machine.

2.1 Spindle test

Spindle thermal growth E_s was tested using a spindle error analyzer manufactured by Lion Precision Corporation, whose maximum testing speed was 60,000 rpm. Following Fig. 2 shows the experimental setup.

Thermal investigation was carried out at 10,000 rpm speed. The spindle rotated at 10,000 rpm for 4 h and then stopped over the next 3 h. The sampling periods for error and temperature data were both set to 10 s. Figure 3 plots the measurement results.

When the spindle rotates temperature and error both increase; then, stopping the spindle causes the temperature and error decrease. Trends approximately follow the exponential

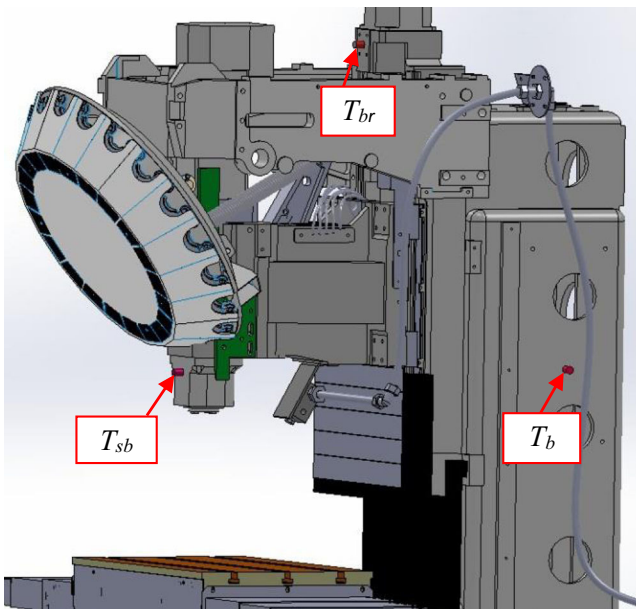

Fig. 1 Positions of temperature sensors on the machine tool

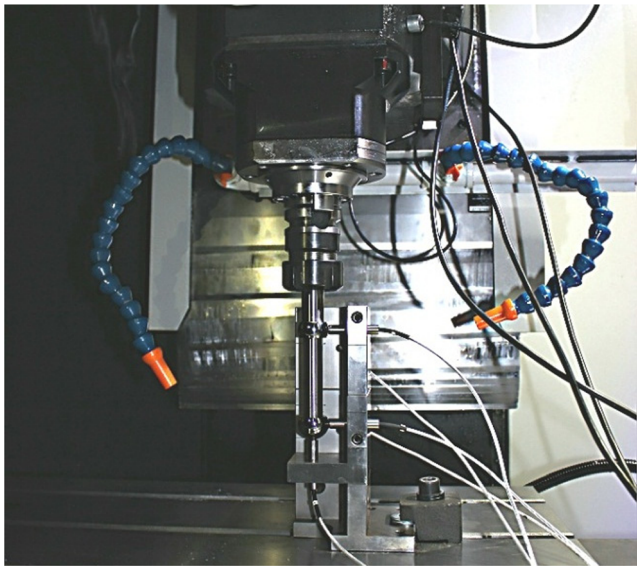

Fig. 2 Experimental setup for measuring spindle thermal growth

law; the correlation between temperature and error seems good, and the calculated correlation coefficient is 0.83.

2.2 Z-axis test

The total servo axis thermal error was divided into the TEE in the stroke range and the TDE of origin. The aforementioned literature reports that most of the studies focused on TEE, while the thermal drift error (TDE) of origin has been rarely studied. Assuming that the nut moves on the screw within the range 0–P_z, the relative distance between the spindle to worktable will change due to thermal errors in Z-direction. On the one hand, the frictional heat of the screw and changes in ambient temperature induce TEE E_{em}. On the other hand, the distance between the origin of servo axis to spindle changes. Because of heat conduction from screw in the stroke range, the heat of bearing block, and ambient temperature variation, E_d appears between the origin of servo axis and spindle. E_{em} depends on position and temperature, E_d only relates to temperature.

Z-axis thermal errors were investigated using a XL80 dual-frequency laser interferometer, and the experimental setup is shown in Fig. 4. To get the real values of positioning errors, the so-called expansion compensation coefficient was set as 20 °C. The experimental setup for measuring Z-axis thermal error is shown in Fig. 4.

The thermal test of Z-axis followed these steps: (1) Test the initial positioning error of the Z-axis in the range from −10 to −290 mm and record the values of T_b and T_{br}. Clearance at the test starting point should be made in the first test. (2) Move the Z-axis in the range from −10 to −290 mm at a speed of 8000 mm/min for a period. (3) Stop moving Z-axis. Test the positioning error and record the values of T_b and T_{br}. (4) Repeat steps (2) and (3) for several times; the achievement of heat balance condition is not necessary. (5) Stop Z-axis at −10 mm position and cool down the machine. Test the positioning error at intervals and record T_b and T_{br} values. Table 1 lists warming-up and cooling-down parameters.

Figure 5 shows the results of Z-axis test.

The figure highlights that the positioning errors in the testing range and the position of test starting point change with the increase of temperature. The tested comprehensive thermal errors of Z-axis were decomposed as follows: the thermal error data of all the tests were processed to make the errors at the first test points as zero, and the E_{em} was obtained; the errors at the first test points of all the tests were extracted to compose E_d. Following Eq. (1) describes the error decomposition.

$$\begin{aligned} E_{em} &= E_{emd}(U,V) - E_{emd}(U,1) \\ E_d &= E_{emd}(U,1) \end{aligned} \tag{1}$$

where E_{em} is thermal expansion error of servo axis; E_d is thermal drift error of origin of servo axis; $E_{emd}(U,V)$ is tested

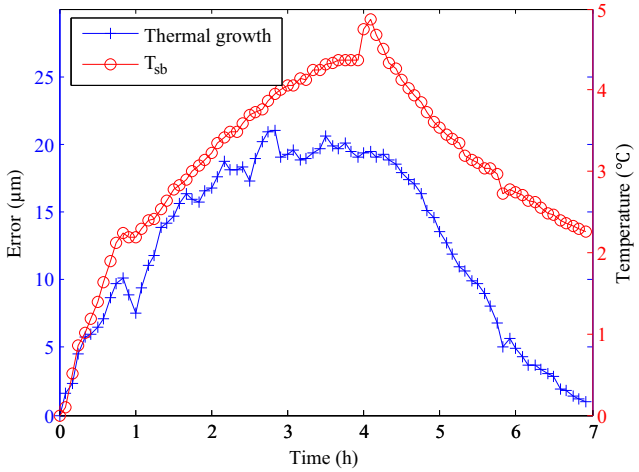

Fig. 3 Spindle thermal growth and temperature

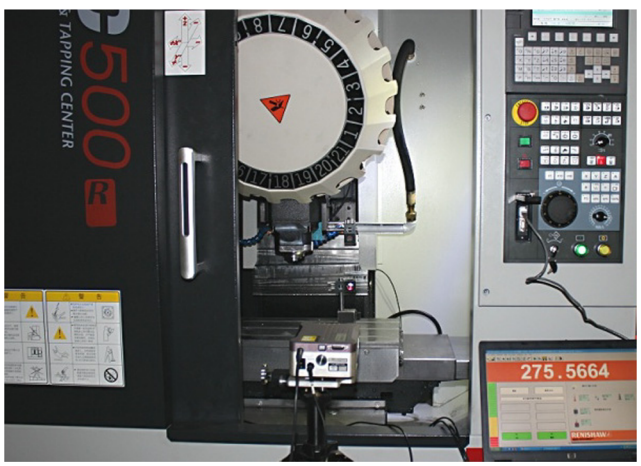

Fig. 4 Investigation of Z-axis thermal error, experimental setup

Table 1 Parameters of thermal error tests

Number	Speed (mm/min)	Range (mm)	Time (min)
State 1	–	–	0
State 2	8000	−10 to −290	10
State 3	8000	−10 to −290	10
State 4	8000	−10 to −290	10
State 5	8000	−10 to −290	10
State 6	0	−10	10
State 7	0	−10	8
State 8	0	−10	10
State 9	0	−10	10
State 10	0	−10	10
State 11	0	−10	12
State 12	0	−10	10

thermal error of Z-axis shown in Fig. 5; U is test times; V is test points of the servo axis.

Figure 6 shows the decomposition of the comprehensive Z-axis thermal error.

The TDE curve shows that TDE increases during warm-up due to the temperature rise of the bearing block and screw; in the cooling-down phase, temperature drop of the bearing block and of the screws cause TDE decreasing. Besides, TDE will also change with the variation of ambient temperature according to theoretical analysis. TDE will decrease when the ambient temperature rises due to the whole machine becomes big; on the contrary, TDE will increase when the ambient temperature falls due to the whole machine becomes small. However, as the time for investigation of thermal errors of servo axis is short and ambient temperature variation is small, it is challenging to observe the influence of ambient temperature on TDE.

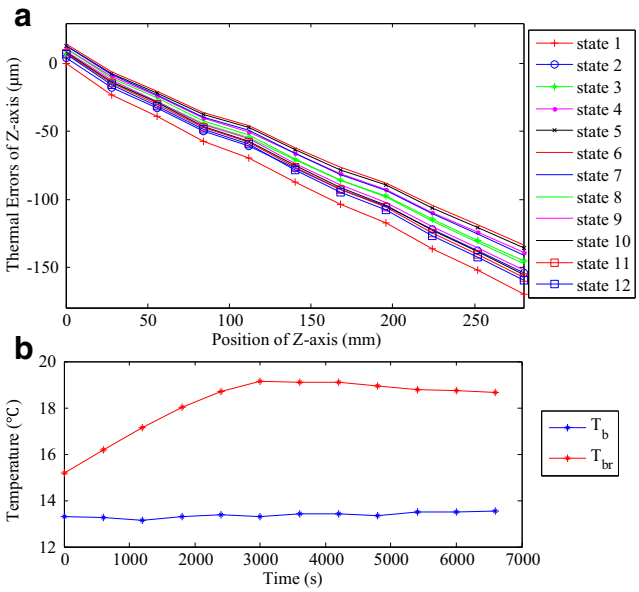

Fig. 5 **a** Thermal errors of Z-axis. **b** Temperatures of Z-axis

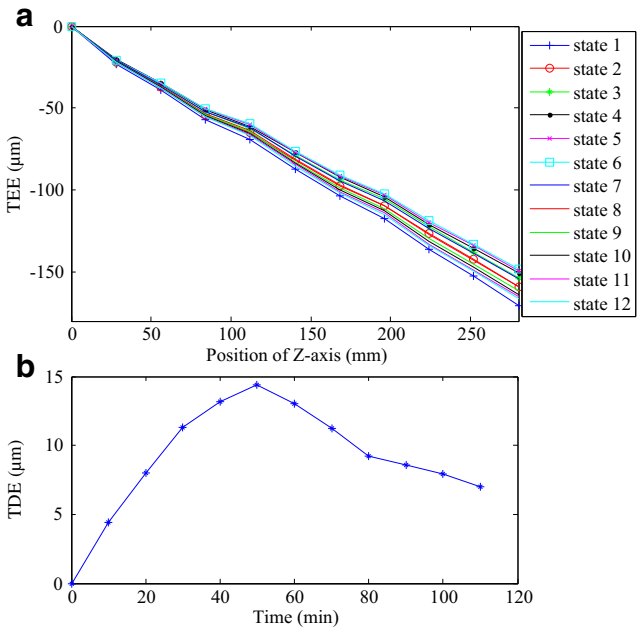

Fig. 6 Decomposition of the comprehensive Z-axis thermal error. **a** TEE. **b** TDE

3 Modeling and parameter optimization

3.1 Combination of spindle and servo axis errors

The comprehensive thermal growth of spindle and servo axis is shown in Fig. 7. Thermal growth of the nut is influenced by both TDE and TEE terms. At the end of spindle, TDE and TEE will superpose and aggravate the axial thermal errors of machine tools; thus, these three types of thermal errors should be summed in actual error compensation.

The thermal tilt error may occur after running the spindle. However, the thermal tilt angle is very small, and the axial thermal growth is almost the same to its projection to Z-direction. Therefore, the expression of comprehensive thermal growth of spindle and servo axis can be expressed as follows:

$$E_{com}(T_{sb}, T_b, T_{br}, P_z) = E_s + E_{em} + E_d \quad (2)$$

where P_z is the position of servo axis; E_s is the thermal growth of spindle.

The comprehensive thermal growth is relative to T_{sb}, T_b, T_{br}, and P_z. Therefore, by acquiring in real time the temperatures of the three sensors and the position of Z-axis, the real-time compensation value can be calculated. Following sections 3.2 and 3.3 introduce the modeling of spindle and servo axis, respectively.

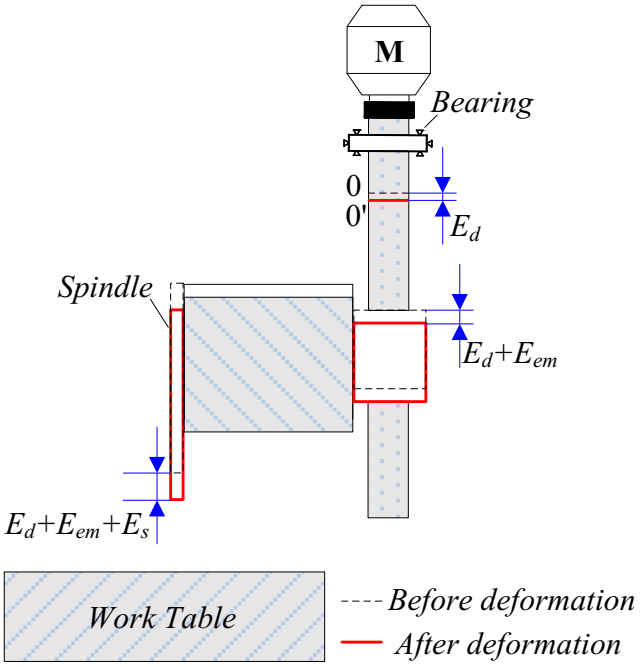

Fig. 7 Comprehensive thermal growth of spindle and servo axis

3.2 Modeling of spindle

Considering the thermal growth curve shown in Fig. 3, it is assumed that the axial thermal growth during rising and falling phase increases and decreases according to the exponential law [5]. In Fig. 8, when the spindle rotates at the speed of n from initial steady state condition, E_s increases exponentially before reaching steady state thermal error E_{sd}. So, thermal growth E_s(t) at any time can be calculated according to Eq. (3) during transient process [5].

$$E_s(t)-E_s(t-1) = (E_{sd}(t-1)-E_s(t-1)) \times \left(1-e^{-\Delta t/\tau}\right) \quad (3)$$

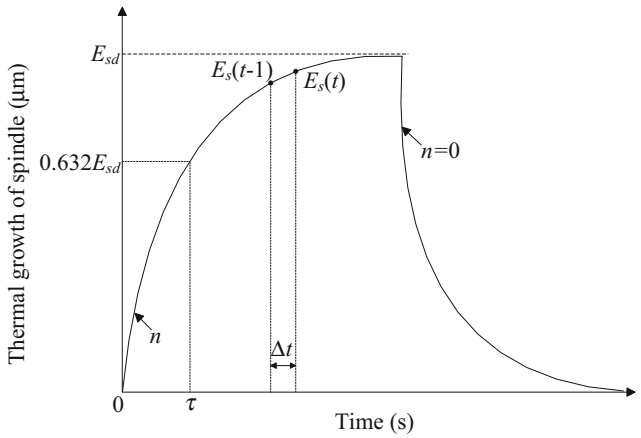

Fig. 8 Spindle thermal growth diagram

where, $E_s(t)$ is the thermal growth at the time of t, τ is the mean time constant of the exponential curve, Δt is the sampling period for thermal errors of spindle, $E_{sd}(t\text{-}1)$ is the steady state thermal error at the time of t-1. Because the spindle rotation speed may change with time, E_{sd} is time dependent.

The change of spindle rotating speed and starting of cooling system may lead to the change of E_{sd} [4]. When the thermal growth does not continue to follow the previous exponential curve because of the change of rotating speed and starting of cooling system, the temperature of spindle will change correspondingly. Therefore, the temperature T_{sb} on the outer surface of the front bearing of spindle is chosen as the temperature reference index. The change in velocity and acceleration of T_{sb} is used for calculating the real-time steady value of the spindle thermal growth E_{sd} in following Eq. (4).

$$E_{sd}(t) = \eta \times \frac{\partial T_{sb}(t)}{\partial t} + \phi \times \frac{\partial^2 T_{sb}(t)}{\partial^2 t} \quad (4)$$

where, $E_{sd}(t)$ is the steady value of thermal growth at time t, $T_{sb}(t)$ is the temperature on the outer surface of the front bearing of spindle at time t, η, and φ are response characteristic coefficients to be identified.

Because high frequency interference exists in the temperature data collected by temperature sensor, the calculated value of thermal growth E_s will contain high frequency interference. Therefore, filtering is essential for the compensation value and it is performed by Eq. (5).

$$G(s) = \frac{E_{sf}}{E_s} = \frac{1}{s+b} \quad (5)$$

where, E_{sf} is calculated spindle thermal growth after filtering, s is Laplace operator, b is the parameter to be identified.

It can be observed that the model based on temperature variation can predict the thermal growth of spindle not only under constant rotation speed but also during the change of rotating speed and starting of cooling system. Therefore, the robustness of the proposed model is strong. This is much better than models based on rotating speed, which is ineffective for randomly starting of cooling system.

The parameters τ, η, φ, and b need to be identified in Eqs. (3)–(5). The optimized values can be obtained from Eq. (6).

$$\begin{aligned} \min[F(\tau,\eta,\phi,b)] &= \sum_{k=1}^{K} \left(E_{sf}(k)-E_{st}(k)\right) \\ s.t. \quad & e_d(1) \le \tau \le e_u(1) \\ & e_d(2) \le \eta \le e_u(2) \\ & e_d(3) \le \phi \le e_u(3) \\ & e_d(4) \le b \le e_u(4) \end{aligned} \quad (6)$$

where, E_{st} is the tested thermal growth, $e_d(i)$ is the lower limitation of the i-th parameter, $e_u(i)$ is the upper limitation of the i-th parameter.

3.3 Modeling of servo axis

3.3.1 TEE model

Because only the axial thermal deformation of screw affects the machining accuracy of machine tools, the screw is simplified to a one-dimensional bar [18] and discretized into M segments, each one length L. The thermal field of a screw is a function not only of position but also of temperature [19]. Moreover, TEE is affected not only by ambient temperature variation but also by the friction heat of nut and screw. According to the temperature superposition principle, they can be superposed [20], that is, the temperature response of multiple sources is equal to the sum of the temperature responses of all the single sources. So, TEE caused by ambient temperature variation and the friction heat of nut and screw are calculated separately [21]:

(1) TEE caused by ambient temperature variation

The error E_e at time t caused by ambient temperature variation in the stroke range is as follows:

$$E_e(t) = \alpha \times (T_b(t) - T_{b0}) \times P_z \tag{7}$$

where, α is the thermal expansion coefficient of screw, μm/(m × °C); $T_b(t)$ is the real-time temperature at time t, °C; T_{b0} is the initial temperature during the test, °C.

(2) TEE caused by the friction heat of nut and screw

For a certain segment L_i of screw, the thermal equilibrium equation can be expressed as follows:

$$c \times (\rho \times L_i \times S) \times (T_{L_i}(t) - T_{L_i}(t-\Delta t)) = Q_{f-L_i}(t) - Q_{c-L_i}(t) - Q_{t-L_i}(t) \tag{8}$$

where, c is screw heat capacity, J/(Kg × °C); ρ is screw density, Kg/m^3; S is equivalent sectional area, m^2; $T_{L_i}(t)$ is temperature of L_i at time t, °C; $Q_{f-L_i}(t)$ is friction heat production of L_i during (t-Δt, t), J; $Q_{c-L_i}(t)$ is heat convection of L_i with surrounding air during (t-Δt, t), J; $Q_{t-L_i}(t)$ is axial heat conduction of L_i to both sides during (t-Δt, t), J.

(1) Frictional heat production

Assuming that Q is the heat production of L_i after one friction, the total frictional heat production $Q_{f-L_i}(t)$. during (t-Δt, t) can be expressed as follows:

$$Q_{f-L_i}(t) = Q \times N \tag{9}$$

where N is the number of friction times of L_i during (t-Δt, t).

(2) Heat convection

The heat convection $Q_{c-L_i}(t)$ during (t-Δt, t) can be expressed as follows:

$$Q_{c-L_i}(t) = h \times S' \times \left(T_{L_i}(t) - T_f(t)\right) \times \Delta t \tag{10}$$

where h is heat exchange coefficient, W/(m^2 × °C); S' is heat exchange area of L_i with the surrounding air, m^2; $T_f(t)$ is ambient temperature and almost the same as T_b, °C.

According to Nusselt criterion, h can be expressed as follows:

$$h = \frac{N_u \times \lambda_a}{L} \tag{11}$$

where N_u is Nusselt number; L is feature size, m; λ_a is heat conduction coefficient of air, W/(m × °C).The Nusselt number N_u under natural convection condition is:

$$N_u = C \times P_r \times \left(\frac{gL^3\beta\Delta T}{\upsilon^2}\right)^m \tag{12}$$

where C and m are coefficients determined by the heat source and airflow form [22]; P_r is Prandtl number; g is gravitational acceleration, m/s^2; β is expansion coefficient of air, °C^{-1}; υ is kinematic viscosity of air, m^2/s; ΔT is temperature difference between air and screw, °C.

(3) Axial heat conduction

The heat passing through the screw cross-section per unit of time is proportional to the temperature variation rate and the screw cross-sectional area:

$$Q_{t-L_i}(t) = \lambda \times S \times \frac{\partial T}{\partial x} = S \times q' \tag{13}$$

where S is screw cross-sectional area, m^2; q' is heat flow density, J/m^2.

Discretizing Eq. (13), the axial heat conduction $Q_{t-L_i}(t)$ during (t-Δt, t) can be expressed as follows:

$$Q_{t-L_i}(t) = \lambda \times S \times \frac{\left(T_{L_i}(t) - T_{L_{i+1}}(t)\right) + \left(T_{L_i}(t) - T_{L_{i-1}}(t)\right)}{L} \times \Delta t \tag{14}$$

In particular, for L^1 and L^M:

$$Q_{t-L_1}(t) = \lambda \times S \times \frac{T_{L_1}(t) - T_{L_b}(t)}{0.5 \times (L_b + L)} \times \Delta t + \lambda \times S \times \frac{T_{L_1}(t) - T_{L_2}(t)}{L} \times \Delta t \tag{15}$$

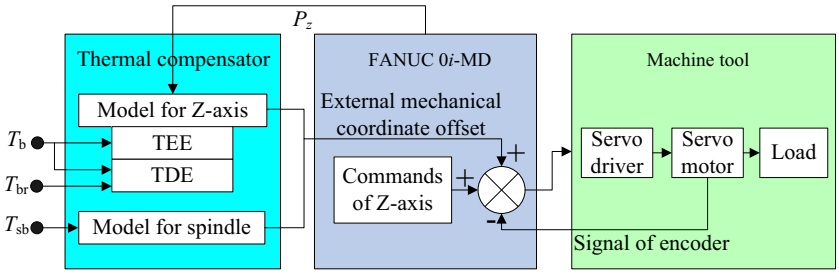

Fig. 9 Illustrative diagram of compensation principle

$$Q_{t-L_M}(t) = \lambda \times S \times \frac{T_{L_M}(t) - T_{L_{M-1}}(t)}{L} \times \Delta t \quad (16)$$

where L^1 is first segment of screw on the side of bearing block; L^M is last segment of screw on the other side; L^b is length of screw between the bearing block and the origin.

Taking Eqs. (9), (10), (14), (15), and (16) into Eq. (8), the real-time temperature variation $T_{L_i}(t)$ of L^i can be obtained.

The thermal expansion errors E^m of a screw caused by the friction heat of nut and screw at time t can be expressed as follows:

$$E_m(t) = \sum_{i=1}^{M} \alpha \times (T_{L_i}(t) - T_b(t)) \times L_i \quad (17)$$

(3) Combination of TEE

The whole TEE of a servo axis caused by ambient temperature variation and the friction heat of nut and screw can be obtained from Eqs. (7) to (17).

$$E_{em}(t) = E_e(t) + E_m(t) \quad (18)$$

Since TEE model records the dynamic process of the thermal field of a screw, even if the moving speed and range of a servo axis change, excellent compensation effect can still be obtained. In fact, the temperature field of a screw at any time can be accurately predicted.

(4) Parameter optimization

In TEE modeling, some parameters are difficult to determine. Taking the heat exchange coefficient h as an example, its calculation is very complex. Thus, a parameter identification method is required to determine the parameters including h, λ, Q, L^b, S, and S′.

ISIGHT software, which can organize the parameter identification process into a uniform frame, was used for parameter optimization [23]. The program for optimization was written in MATLAB, using following optimization objective function:

$$\min[F(h, \lambda, Q, L_b, S, S')] = \sum_{u=1}^{U} \sum_{v=1}^{V} (E_{em}(u,v) - E_{emt}(u,v)) \quad (19)$$

where $E_{emt}(u, v)$ is servo axis tested thermal error of the v-th test point during the u-th test; $E_{em}(u, v)$ is calculated servo axis thermal error of the v-th test point during the u-th test.

3.3.2 TDE model

The TDE of the servo axis tested in section 2.2 actually reflects the change in distance between the worktable and spindle at the test starting point. The deviation is not only induced by the thermal expansion of screw between the motor-side bearing block and the origin point, which is influenced by ΔT_{br} and ΔT_{L_1} but also induced by the change in ambient temperature ΔT_b. Assuming that E_d is linearly related to ΔT_{br}, ΔT_{L_1} and ΔT_b, the model for E_d can be expressed as follows:

$$E_d = a_1 \Delta T_{br} + a_2 \Delta T_{L_1} + a_3 \Delta T_b + a_4 \quad (20)$$

where a_1, a_2, a_3, and a_4 are coefficients to be identified.

a_1, a_2, a_3, and a_4 can be solved by the least square method. The rise of bearing block and screw will lead to positive TDE,

Fig. 10 Experimental compensation verification test

Table 2 Parameters in compensation tests

State	Servo axis		Rotating speed (rpm)	Time (min)
	Speed (m/min)	Range (mm)		
State 1	10	−10 to −290	8000	10
State 2	8	−10 to −290	8000	10
State 3	10	−50 to −290	9000	10
State 4	8	−50 to −290	9000	10
State 5	10	−30 to −270	10,000	10
State 6	12	−30 to −270	10,000	10
State 7	10	−10 to −290	11,000	10
State 8	0	−10	0	10

while the rise of ambient temperature will turn TDE to become negative. So, the objective function and constraint condition can be expressed by Eq. (21).

$$\begin{aligned} \min[F(a_1,a_2,a_3,a_4)] &= (E_d(T_{br},T_b)-E_{dt}(T_{br},T_b)) \\ s.t. \quad & a_1 > 0 \\ & a_2 > 0 \\ & a_3 < 0 \end{aligned} \tag{21}$$

4 Experiments

4.1 Tests

External mechanical coordinate offset was used for writing compensation values for FANUC 0*i*-MD numerical controller [3]. Thermal compensator and FANUC 0*i*-MD communicated through Ethernet. The compensation principle is shown in Fig. 9.

The compensation for comprehensive thermal growth of spindle and Z-axis was verified using a laser interferometer XL80, as shown in Fig. 10. The experiment followed these steps:

(1) Test the initial positioning error of Z-axis in the range from −10 to −290 mm with and without compensation, respectively. Clearance at the test starting point should be made in the first test.
(2) Let the spindle and Z-axis run according to the information of following Table 2.
(3) Stop and test the positioning error with and without compensation, respectively. Clearance at the test starting point should not be made.

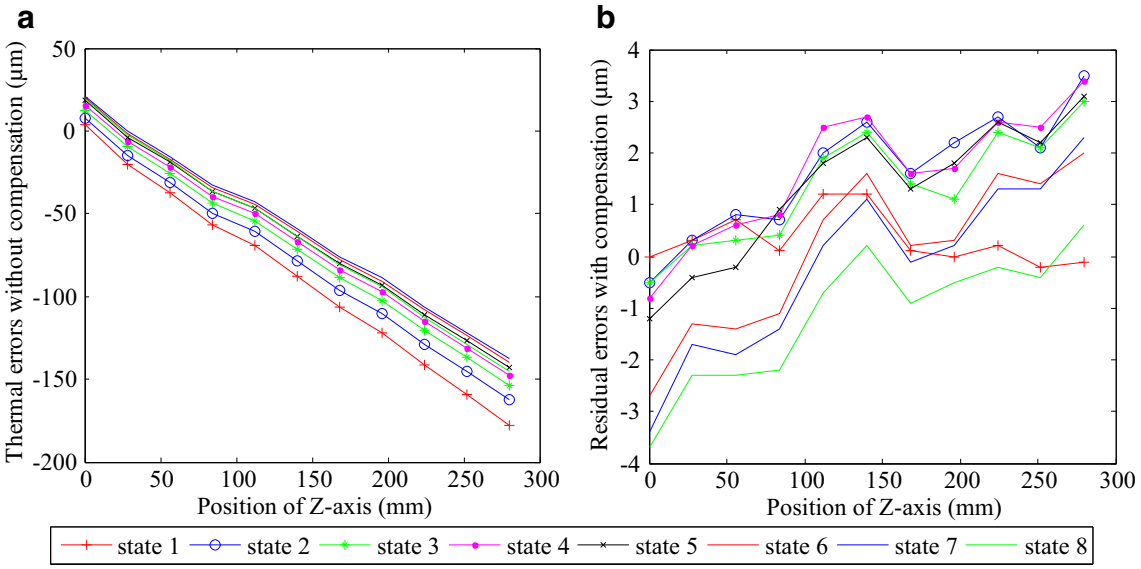

Fig. 11 Thermal growth errors. **a** Without compensation. **b** With compensation

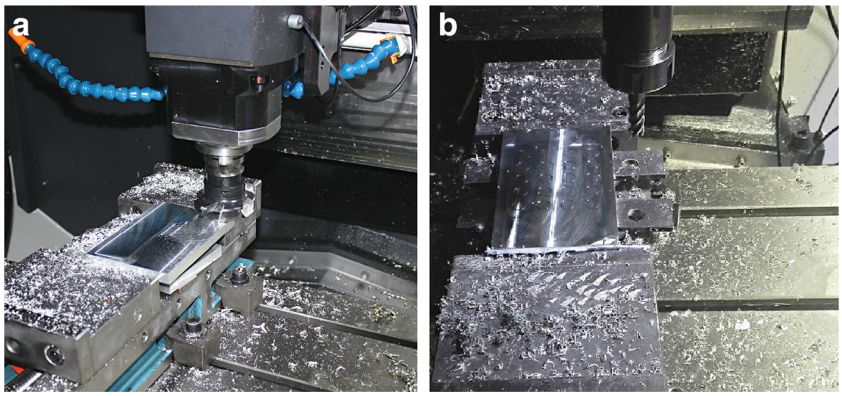

Fig. 12 **a** Milling flat. **b** Drilling holes

(4) Repeat steps (2) and (3) for eight times.

Figure 11 shows the results obtained with and without compensation: the sum of Z-axis positioning error and comprehensive thermal errors of spindle and Z-axis varies from −177.8 to 21.2 μm within the whole stroke range of Z-axis without compensation. After compensation, the total error varies from −3.7 to 3.5 μm, thus proving the high accuracy of the suggested model. In particular, even changing the motion information according to parameters listed in Table 2, the residual errors after the compensation were always small and the strong robustness of the suggested model was assessed.

4.2 Machining test

Machining tests with and without compensation were performed for further verification of the proposed method, and this section presents main results. Temperature sensors were installed on the machine as in Fig. 1. The upper surface of a rectangular workpiece was drilled to observe the differences with and without compensation to the unaided eye.

The machining process was as follows:

(1) The upper surface was milled using a 140-disc milling cutter to ensure surface finished and flat, as shown in Fig. 12a.
(2) Two holes 5 μm depth were drilled without compensation on the left side of the piece by a 20-disc 4-edge milling cutter. Compensation started and two holes −65 μm depth were drilled by the same cutter to the right. Since the Z-axis positioning error was very big, the compensator compensated it. Therefore, a depth of −65 μm is used to avoid the holes with compensation to be too deep.
(3) The worktable moved to the left side and the spindle and Z-axis warmed up (according to Table 1).
(4) Warm up stopped and the worktable moved 18 mm along Y direction. Two holes 5 μm depth were drilled on the left side of the piece without compensation. Then, compensation started and two new holes −65 μm depth were drilled on the right side.
(5) Steps (3) and (4) repeated until five groups of holes were all machined, as shown in Fig. 12b.

Figure 13 shows the workpiece after machining.

Figure 13 shows that the micron-scale error of Z-axis of the vertical drilling center is visible to the unaided eye. Moreover, even if the machine moved according to the parameters listed in Table 3, the accuracy stability with compensation was much better than that without compensation, proving the effectiveness of the proposed model for comprehensive thermal growth compensation.

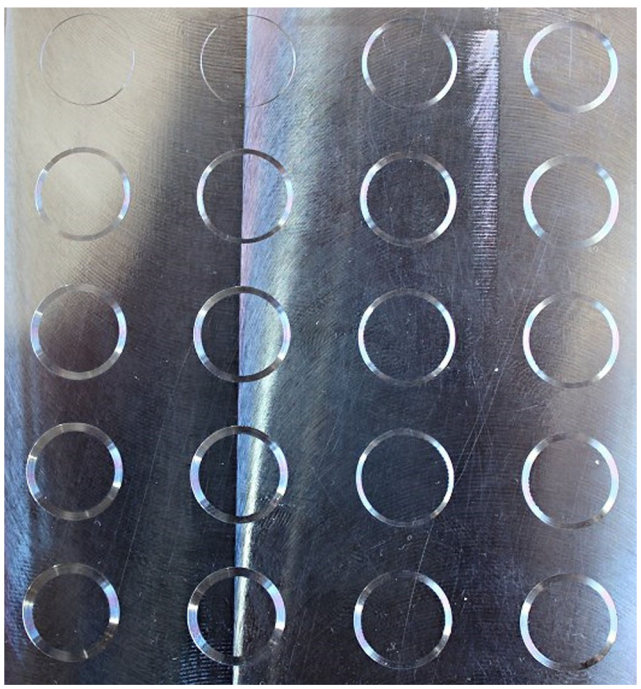

Fig. 13 The machined workpiece

Table 3 Parameters in machining

No.	Z-axis speed (m/min)	Z-axis range (mm)	Spindle rotating speed (rpm)	Time (min)
1	8000	−50 to −290	8000	10
2	9000	−30 to −270	10,000	13
3	10,000	−10 to −250	10,000	13
4	12,000	−10 to −290	11,000	15

5 Conclusions

The modeling method for comprehensive thermal growth of spindle and servo axis was introduced. The experimental and machining test results showed that the accuracy stability with compensation is much higher than that without compensation. Besides, the main advantage of the proposed model is the strong robustness. Therefore, this method can be widely used on machine tools in a non-controlled temperature workshop.

Acknowledgments The authors gratefully acknowledge the support of China Postdoctoral Science Foundation Grant (2015M581400). Moreover, the authors thank the anonymous referees and editor for their valuable comments and suggestions.

References

1. Robert BA (1996) War against thermal expansion. Manuf Eng 116(6):45–50
2. Yang J, Shi H, Feng B, Zhao L, Ma C, Mei XS (2015) Thermal error modeling and compensation for a high-speed motorized spindle. Int J Adv Manuf Technol 77(5–8):1005–1017
3. Fu JZ, Chen ZC (2004) Research on identification of thermal dynamics characteristics parameter of precision machine based on singular value decomposition. J Zhejiang Univ: Eng Sci 38(4): 474–476
4. Liu K, Sun M, Wu Y, Zhu T (2015) Thermal Error Modeling Method for a CNC Machine Tool Feed Drive System. Math Probl Eng 436717
5. Creighton E, Honegger A, Tulsian A, Mukhopadhyay D (2010) Analysis of thermal errors in a high–speed micro–milling spindle. Int J Mach Tools Manuf 50:386–393
6. Lei CL, Rui ZY (2012) Thermal error modeling and forecasting based on multivariate autoregressive model for motorized spindle. Mech Sci Technol Aerospace Eng 31(9):1526–1529
7. Wu CW, Tang CH, Chang CF, Shiao YS (2011) Thermal error compensation method for machine center. Int J Adv Manuf Technol 59:681–689
8. Zhang Y, Yang JG (2011) Modeling for machine tool thermal error based on grey model preprocessing neural network. J Mech Eng 47(7):134–139
9. Li YQ, Yang JG, Zhang HT, Tong HC (2006) Application of grey system model to thermal error modeling on machine tools. China Mech Eng 17(23):2439–2442
10. Shu QL, Li YL, Lv YS (2012) Application of time series analysis to thermal error modeling on NC micro-grinder. Modular Mach Tool Autom Manuf Tech 12:30–32
11. Li YX, Tong HC, Cao HT, Zhang HT, Yang JG (2006) Application of time series analysis to thermal error modeling on NC machine tool. J Sichuan Univ 38(2):74–78
12. Yang H, Ni J (2005) Dynamic neural network modeling for nonlinear, nonstationary machine tool thermally induced error. Int J Mach Tools Manuf 45:455–465
13. Zhu J, Ni J, Shih AJ (2008) Robust machine tool thermal error modeling through thermal mode concept. J Manuf Sci Eng 130: 0610061–0610069
14. Pajor M, Zapłata J (2011) Compensation of thermal deformations of the feed screw in a CNC machine tool. Int J Adv Manuf Technol 35: 9–17
15. Jin ZF, Wang P (2012) Neural network–based thermal error modeling in ball screw. Modular Mach Tool Autom Manuf Tech 1:67–70
16. Ozkan MT (2013) Experimental and artificial neural network study of heat formation values of drilling and boring operations on Al 7075 T6 workpiece. Indian J Eng Mater Sci 20: 259–268
17. Lin WQ, Fu JZ, Chen ZC, Xu YZ (2009) Modeling of NC machine tool thermal error based on adaptive best-fitting WLS-SVM. J Mech Eng 45(3):178–182
18. Chen C, Qiu ZR, Li XF, Dong CJ, Zhang CY (2011) Temperature field model of ball screws used in servo systems. Opt Precis Eng 19: 1151–1158
19. Liu B J (2013) Temperature field and thermal deformation of feed system on gantry machining center. Dissertation, Nanjing University of Aeronautics and Astronautics
20. Xia JY, Wu B, Hu YM (2008) The thermal dynamic characteristic of ball-screw under the variational multi-thermal source. Chin Mech Eng 19(18):955–958
21. Liu K, Liu Y, Sun M, Wu Y, Zhu T (2015) Comprehensive thermal compensation of the servo axes of CNC machine tools. International Journal of Advanced Manufacturing Technology Int J Adv Manuf Technol 1–14
22. Zhang JZ, Chang HP (2009) Heat transfer. Science Press, Beijing
23. Wei W, Qu JY, Wu JY, Yan QD (2011) Research on optimization method for shift schedule of tracked vehicle with hydrodynamic—mechanical transmission. Acta Armamentarii 32:403–407